Universiteit
Leiden
The Netherlands

A computational study of structural and excitonic properties of chlorosomes

Li, X.

Citation
Li, X. (2020, May 6). *A computational study of structural and excitonic properties of chlorosomes*. Retrieved from https://hdl.handle.net/1887/87570

Version:	Publisher's Version
License:	Licence agreement concerning inclusion of doctoral thesis in the Institutional Repository of the University of Leiden
Downloaded from:	https://hdl.handle.net/1887/87570

Note: To cite this publication please use the final published version (if applicable).

Cover Page

Universiteit Leiden

The handle http://hdl.handle.net/1887/87570 holds various files of this Leiden University dissertation.

Author: Li, X.
Title: A computational study of structural and excitonic properties of chlorosomes
Issue Date: 2020-05-06

CHAPTER 4

Dynamic Disorder Drives Exciton Transfer in Tubular Chlorosomal Assemblies

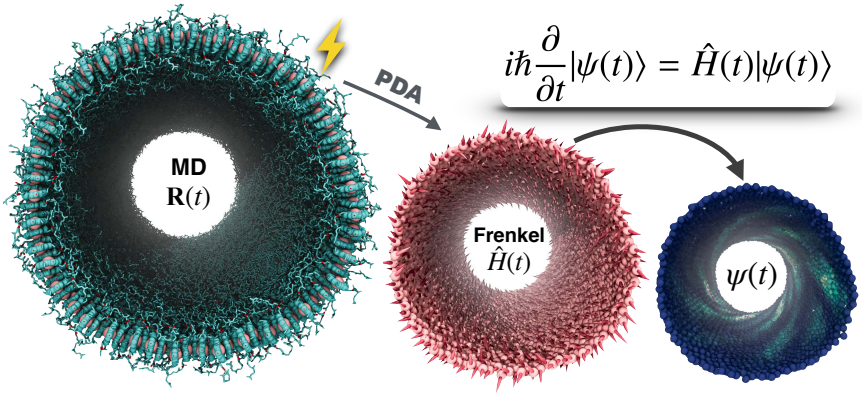

This chapter was submitted as: Xinmeng Li, Francesco Buda, Huub J.M. de Groot, and G. J. Agur Sevink, Dynamic Disorder Drives Exciton Transfer in Tubular Chlorosomal Assemblies, 2020.

Chlorosomes stand out for their highly efficient excitation energy transfer (EET) in extreme low light conditions. Yet, little is known about the EET when a chlorosome is excited to a pure state that is an eigenstate of the exciton Hamiltonian. In this work, we consider the dynamic disorder in the intermolecular electronic coupling explicitly by calculating the electronic coupling terms in the Hamiltonian using nuclear coordinates that are taken from molecular dynamics simulation trajectories. We show that this dynamic disorder is capable of driving the evolution of the exciton, being a stationary state of the initial Hamiltonian. In particular, long-distance excitation energy transfer between domains of high exciton population and oscillatory behavior of the population in the site basis are observed, in line with two-dimensional electronic spectroscopy studies. We also found that in the high exciton population domains, their population variation is correlated with their overall coupling strength. Analysis in a reference state basis shows that such dynamic disorder, originating from thermal energy, creates a fluctuating landscape for the exciton and promotes the EET process. We propose such dynamic disorder as an important microscopic origin for the high efficient EET widely observed in different types of chlorosomes, bio-inspired tubular aggregates, or other light-harvesting complexes.

4.1. Introduction

The survival of green sulfur bacteria in extreme low-light condition relies on the efficiency of their light-harvesting antenna, chlorosomes, which are assemblies of hundreds or thousands bacteriochlorophylls (BChls) pigments.[11–16] Elucidating the design principles behind the efficient excitation energy transfer (EET) that takes place in chlorosomes will contribute to our understanding of photosynthesis[1,2,6,17–24] and may help to develop artificial light-harvesting[25–28] or other optoelectronic devices.[29–32] In spite of recent progress in theoretical and experimental understandings of exciton dynamics in chlorosome systems,[36,40,41,43,44,79,80,84,105,120,121,124,141,146,147] a microscopic origin of efficient EET remains unclear.

Previously in Chapter 2, we identified a rotational degree of freedom that is prominent even though the pigments are densely packed together. This

head-head rotational dynamics between neighboring pigments is expected to affect their electronic couplings (see Chapter 3).[18] Introducing such rotational disorder in the Frenkel Hamiltonian is found to induce delocalization of exciton states. Optically active states near to the bottom of the exciton band are found to be composed of scattered domains of population density that are distributed over the whole tube (Chapter 3). By analyzing the manifold of exciton states along a MD trajectory of molecular conformations, we found level crossings between states and high sensitivity of the exciton state domain patterns to the dynamic disorder. This may induce long-distance exciton transfer between scattered domains involving different exciton states (Chapter 3), in line with 2D electronic spectroscopy (2DES) studies.[84,120] Beyond our previous treatment, here we conducted quantum dynamics simulations of exciton evolution, investigate the effect of the rotational dynamic disorder on the exciton density matrix, and show that it rapidly converts a pure state generated by optical excitation at the start of the trajectory into a superposition state characterized by many nonzero off-diagonal elements (a.k.a. coherences) in the density matrix. Considering that such dynamic disorder is also shared by artificial tube assemblies[48–50] with proven efficient exciton transport ability, we propose thermally induced quantum instability by rapid molecular dynamics, faster than the quantum decoherence, and starting from a pure quantum state as a promising microscopic origin of efficient EET beyond the Born-Oppenheimer regime where the electronic motion follows the nuclear dynamics.

Apart from the previous lack of a precise chlorosome structure, the study of exciton evolution in chlorosomes has been hampered by the large dimension of these assemblies, which rule out any full quantum treatment.[73,75,77,148] In line with previous treatments,[36,40,41,43,44,71,79,80] we therefore consider an effective model, a Frenkel Exciton Hamiltonian, as a starting point. Fujita *et al.*[40,43] used such a Hamiltonian to study the exciton dynamics of a stacked-ring structure, adding stochastic fluctuations to the site energies, comparing the exciton diffusion under different types of fluctuations. Márquez *et al.*[105] studied the exciton dynamics for different lattice models of chlorosomes. They introduced site energy variation through exciton-phonon interactions. Upon exciting a single site in the system, these studies all observed exciton diffusion to the whole tube within a ps time. In systems more complicated than a single tube structure, other types of non-stationary initial conditions were also considered.[41,44]

Based on our recent progress in constructing chlorosome structures that satisfy experimental constraints in terms of microscopic detail (see Chapters 2 and 3), we are capable of studying the exciton dynamics of realistic chlorosomes within the standard Frenkel Exciton treatment. We exploit the nuclear coordinates taken from ground state molecular dynamics trajectories to derive time-dependent electronic coupling terms in the exciton Hamiltonian, thereby including the dynamic disorder explicitly. In line with the low light conditions and in contrast to previous studies,[40,41,43,44,105] we select the exciton eigenstate of the Hamiltonian with the largest oscillator strength as the initial pure state, *i.e.* at $t = 0$, from which we start our simulation.[149] Since the initial state is stationary, the evolution of the exciton is fully driven by the dynamic disorder. As a first step towards fully understanding functional mechanisms of chlorosomes, we studied the exciton dynamics in a quasi-closed system manner. While the classical trajectories involve coupling to a heat bath with a thermostat, the propagation is performed in a series of closed quantum system simulations, without including energy dissipation or a sink for the exciton. The dynamic disorder parametrically included in $\hat{H}(t)$ is able to introduce both the population variation in the state basis and substantial coherences between exciton states on a time scale < 100 fs, which we consider sufficiently fast to overcome quantum dephasing and contribute to driving long range exciton transport.

4.2. Computational Methods

We conducted all-atom molecular dynamics (MD) simulations to obtain the nuclear coordinates along a trajectory, and used these coordinates to extract time-dependent spatial information of the transition dipole vectors $\boldsymbol{\mu}(t)$ and their positions $\mathbf{R}(t)$ (see Figure C.1 and computational details in Appendix C). Following our previous work (Chapter 3), we considered full tube structures purely composed of BChl *c* molecules, which means that static disorder stemming from chemical compositions and structural defects are not included in our treatment. Given these spatial properties $\{\boldsymbol{\mu}(t), \mathbf{R}(t)\}$, the Frenkel Exciton

Hamiltonian is calculated by

$$\hat{H}(t) = \sum_i \nu \, |i\rangle\langle i| + \sum_{i \neq j} J_{ij}(\boldsymbol{\mu}_i(t), \boldsymbol{\mu}_j(t), \mathbf{R}_{ij}(t)) \, |j\rangle\langle i| \qquad i, j \in [1, N] \tag{4.1}$$

where diagonal terms ν represent the monomer excitation energy of a BChl *c* pigment molecule, and the off-diagonal terms J_{ij} represent the electronic coupling between molecules i and j, which is calculated via the standard point-dipole approximation (PDA)

$$J_{ij}(\boldsymbol{\mu}_i(t), \boldsymbol{\mu}_j(t), \mathbf{R}_{ij}(t)) = \frac{\boldsymbol{\mu}_i \cdot \boldsymbol{\mu}_j}{\left|\mathbf{R}_{ij}\right|^3} - 3\frac{(\boldsymbol{\mu}_i \cdot \mathbf{R}_{ij})(\boldsymbol{\mu}_j \cdot \mathbf{R}_{ij})}{\left|\mathbf{R}_{ij}\right|^5}. \tag{4.2}$$

Site energies. Although chlorosomes exhibit gross structural heterogeneity at the supramolecular level, they are remarkably homogeneous at the molecular level. First, solid state NMR studies on mutant and WT chlorosomes have consistently revealed two well defined structural fractions.[37] Second, fluorescence excitation spectroscopy measurements for individual chlorosomes by Günther *et al* have confirmed the presence of two well-defined components with very little difference in the average site energies of $\Delta E_{12} = 34$ cm^{-1} and limited inhomogeneous broadening.[45] The energies of the exciton states appear to shift primarily due to variation of the curvature of tubular assemblies.[45] For a simulated tube of 7.5 nm diameter and with identical site energies for the building blocks, we obtain a total inhomogeneous width of 60 cm^{-1} due to curvature, which is in line with experimental data that also show static optical broadening in the tubes, while the underlying MAS NMR data reveal high, nearly crystalline homogeneity at the molecular level.[45] Third, in Chapter 2 we found converging evidence that the two components are due to molecules with and without interstack hydrogen bonding. Since the difference in the energies for the lower exciton states are very minor according to the fluorescence excitation data, the direct effect of the environment, including the variation in hydrogen bonding, on the site energies is very small. To simulate these experimentally determined characteristics, the site energies, represented by the diagonal terms in Hamiltonian, were set to a fixed value $\nu_i = \nu = 15390$ cm^{-1} that is the same for all molecules, while the electronic coupling between molecules (off-diagonal terms in Hamiltonian) are parameterized according to conformations and supramolecular structure taken from MD trajectories, which includes both

the molecular rotations and the curvature. More discussions of our choices are available in Chapter 3.

Such a treatment of $\hat{H}(t)$ gives rise to dynamic disorder in the electronic coupling microscopically obtained from the ground state molecular dynamics. Details about the MD simulation setup and Hamiltonian parameterization are available in the Appendix C. The evolution of the exciton wave function is governed by the time-dependent Schrödinger equation

$$i\hbar\frac{\partial}{\partial t}|\psi(t)\rangle = \hat{H}(t)|\psi(t)\rangle \tag{4.3}$$

For optimal computational efficiency, the time-dependent Hamiltonian $\hat{H}(t)$ is updated discretely every short time interval Δt according to the corresponding nuclear positions and is assumed constant in between updates on the Δt time intervals.[82,83] A requirement in such a strategy is that Δt is small enough, meaning that each update only introduces a relative small perturbation to the Hamiltonian from the previous interval. Considering the relative motions between molecules are slower than intra-molecule vibrational modes, we select $\Delta t = 20$ fs. In particular, we found that the difference in nuclear positions between structures at $t = 0$ and $t = 20$ fs is quite small (≈ 0.1 Å), see details in later discussions. Furthermore, we take the Hamiltonian $\hat{H}_1 = \hat{H}(t = \Delta t)$ and investigated the exciton dynamics for this constant Hamiltonian, which is referred to as the static case $\hat{H}_1$ in later discussions. As shown later, the exciton evolution in the static case $\hat{H}_1$ is very weak, which confirms that the perturbation to the Hamiltonian $\hat{H}_0$ at $t = 0$ is indeed small. We conclude that the $\Delta t = 20$ fs is small enough in this study. Such an updating strategy is also adopted and discussed in Chapter 3. Since both the Hamiltonian $\hat{H}(t)$ and exciton wave function $|\psi(t)\rangle$ are formulated in the site basis, $|\psi(t)\rangle$ is propagated directly, with a time step of 1 fs, through solving the time-dependent Schrödinger equation (eq 4.3) using the "zvode" ODE solver implemented in the QUTIP package.[150,151] Due to the discrete nature of $\hat{H}(t)$ in our treatment, $|\psi(t)\rangle$ is propagated step-wise.

The detailed propagation sequence is provided in the Scheme C.1. We take as the initial wave function $|\psi(0)\rangle$, *i.e.* the eigenstate of the Hamiltonian $\hat{H}_0 = \hat{H}(t = 0)$ with the largest oscillator strength. This choice corresponds to a situation in which the chlorosome absorbs one photon in low light conditions.

In contrast to previous studies, we particularly did not choose an initial wave function fully localized at one molecular site, because light excites eigenstates rather than individual molecules.[149,152] The exciton dynamics trajectory is a collection of $|\psi(t)\rangle$ in the site basis. For any given wave function $|\psi(t)\rangle$, the density matrix $\rho(t)$ in the site basis is obtained as

$$\rho(t) = |\psi(t)\rangle\langle\psi(t)| = \sum_{i=1}^{N}\sum_{j=1}^{N}\rho_{ij}(t)\,|i\rangle\langle j| \tag{4.4}$$

where $\rho_{ij}(t)$ describes the populations ($i = j$) and coherences ($i \neq j$) in the site basis. To clearly characterize the non-stationary nature of the exciton dynamics, we further performed analysis in the state basis $|\phi_k\rangle$,which are the eigenstates of the Hamiltonian at $t = 0$, $\hat{H}_0\,|\phi_k\rangle = \varepsilon_k\,|\phi_k\rangle$. The density matrix ρ^{ϕ} in the state basis $|\phi_k\rangle$, is calculated from the density matrix in the site basis as

$$\rho^{\phi}(t) = P^{-1}\rho(t)P \tag{4.5}$$

where P is the projection matrix composed of the column vectors for states in the state basis $|\phi_k\rangle$. The density matrix $\rho^{\phi}_{kl}(t)$ now describes the populations ($k = l$) and coherences ($k \neq l$) in the reference state basis $|\phi_k\rangle$. In addition, we also projected the density matrix $\rho(t)$ to the state basis of $\hat{H}(t)$ after each update, see more details in Scheme C.1.

4.3. Results and Discussion

We conducted simulations of the exciton dynamics for both single tube and multi-tube structures. Most results consider the single tube system, which we used to investigate how the initial eigenstate evolves, and whether long-distance exciton transfer can take place purely driven by dynamic disorder. The multi-tube system is mainly considered to focus on the effect of hierarchical structure on the inter-tube exciton transfer.

Single Tube Setup. Figure 4.1 illustrates relevant details of the tube structure, together with the initial wave function used in the exciton dynamics simulation. Following our static analysis in Chapter 3, we selected a 60 nm long tube with

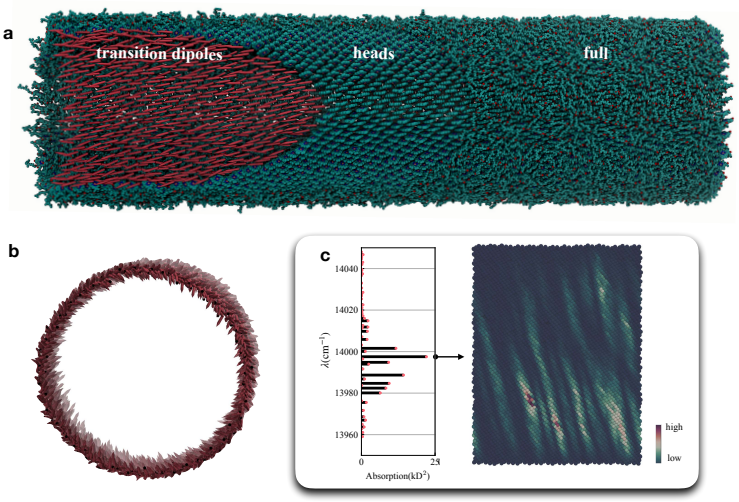

Figure 4.1: Representative images of the tubular structure and the exciton state of largest oscillator strength for a single chlorosomal tube assembly. (a) Atomistic structure. The tube is composed of 4547 BChl *c* molecules, with radius $R = 7.5$ nm and length $L = 60$ nm. Transition dipoles and heads of BChl *c* molecules are highlighted by removing covering atoms. (b) Orthonormal projection of all the transition dipoles in the whole tube, showing considerable disorder in their relative orientations. (c) Absorption spectrum of the tube (left) and spatial distribution the exciton state of largest oscillator strength (right). The wave function is projected on a plane unrolled from the tube structure, see Figure C.2 for other types of visualization.

a chiral angle of 49.6°, which matches optical spectra found in experiments. After equilibration, molecular conformations are collected every $\Delta t = 20$ fs along a 1 ps MD trajectory to determine $\{\boldsymbol{\mu}(t), \mathbf{R}(t)\}$ and consequently the Hamiltonian $\hat{H}(t)$ (Eq.4.1). We refer to Chapter 3 for the details about the variation of exciton states in different molecular conformations along such a MD trajectory. The root mean square displacement RMSD that relates to nuclear coordinates that define the transition dipole, shows that the structural deviation from the initial tube continuously grows on the considered time scale of 1 ps, whereas the RMSD at $t = 20$ fs is quite small (≈ 0.1 Å), indicating that the perturbation $\Delta\hat{H}$ in $\hat{H}_1 = \hat{H}_0 + \Delta\hat{H}$ is indeed quite small, see Figure C.3 for more details. As can be seen from the snapshots in Figure 4.1a–b, varying molecular orientations produce considerable rotational disorder in the transition dipoles. We calculated the absorption spectrum for $\hat{H}_0$, and selected the eigenstate with the largest absorption probability (state number $k = 20$) as the initial exciton wave function $|\psi(0)\rangle$ in the exciton dynamics simulation. As Figure 4.1c shows, disorder in the electronic coupling suppresses exciton delocalization and leads to a few small domains of high exciton population.

Enhancement of Exciton Transport by Dynamic Disorder. In order to quantify transport away from the initial state, we compute the survival probability $P_S(t) = |\langle\psi(0)|\psi(t)\rangle|^2$ of the initial state,[82] defined as the squared of the overlap integral between the initial wave function and the wave function at time t, see Figure 4.2. For the static case, $\hat{H}_1$, the exciton stays close to the original state as P_S is still significant after 1 ps, with $P_S > 0.9$ along the whole trajectory. For the dynamic case, $\hat{H}(t)$, P_S decreases substantially, with $P_S < 0.3$ at 1 ps. The abrupt changing of the power law behavior of P_S around 200 fs highlights the role of the dynamic disorder in exciton transfer: the original pure state changes into a mixed state due to the changing Hamiltonian.

For the $\hat{H}(t)$ case, a significant variation of the spatial distribution of the wave functions is observed, accompanying the decrease of P_S, as shown in Figure 4.2b (selected snapshots) and Movie S1 [†]. Tracing domains of high exciton population, for instance, the domains I – III labeled in Figure 4.2b, we observed the presence of (long-distance) exciton energy transfer between such domains. This observation is in line with experimental studies[120] and our previous static

[†]Movie S1-S6 (MP4) files in `chapter_4` folder at https://github.com/xinmeng2015/chlorosome_phd_thesis or https://doi.org/10.5281/zenodo.3674742

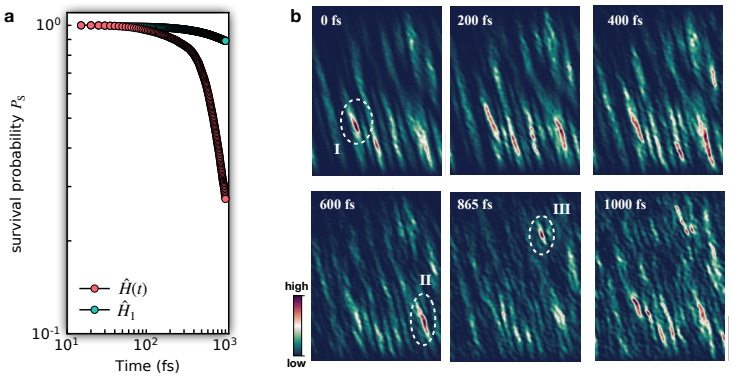

Figure 4.2: Enhancement of exciton dynamics due to dynamic disorder from MD. (a) Comparison of the survival probability P_S of the initial exciton state in case $\hat{H}(t)$ and case $\hat{H}_1$. (b) Spatial distribution of the exciton at selected times in the $\hat{H}(t)$ case. Three domains I–III are labeled to illustrate the long distance migration. See Movie S1 and Movie S2 for the comparison of whole 1 ps exciton dynamics trajectories in the two cases.

analysis in Chapter 3. The substantial variation of the exciton within the short time of 1 ps is also in line with intra-chlorosome exciton transfer time scales (below 1 ps) observed in experimental works.[84,120,121,124,141,147]

We may relate these observations to photosynthetic bacteria where excitonic energy initially captured in chlorosome antennae needs to migrate to the baseplate within a few ps before exciton annihilation occurs.[61] We note that during the energy transfer process, a spatial barrier may be present, meaning that the initial state, or a low energy state where an exciton might be trapped, is spatially remote from the target state that is localized at the baseplate. We illustrated such a situation in Scheme C.2. In the static case, $\hat{H}_1$, such a spatial barrier will delay or even prohibit the exciton transfer process, as the exciton is trapped in the initial state and the spatial sampling of the exciton is limited (see Movie S2 [†]). Introducing dynamic disorder, as shown in the $\hat{H}(t)$ case, renders the exciton capable of dynamically sampling the whole extent of the tube within the characteristic intra-chlorosome transfer timescale of 1 ps.[61] As summarized in Scheme C.2, dynamic disorder may introduce "intermediate" domains that are close to the baseplate and helps the following energy transfer.

From the perspective of energy transfer, the exciton dynamics in our $\hat{H}(t)$ case belongs to a coherent regime, *i.e.* the regime where energy transfer is perceived as fastest, for which the standard Förster and Redfield theories do not apply.[20] Such coherent excitation energy transfer is well-recognized in photosynthetic systems. In such a process, the exciton diffusion equation can be described in terms of a coherent part and an incoherent part.[153–155] Since our initial exciton state is stationary, there is initially no coherence between exciton states. Each update of the Hamiltonian $\hat{H}(t)$ will disturb the coherent evolution in the previous period (incoherent contribution), and at the same time it introduces new coherences (coherent contribution).[155] This illustrates the complexity of energy transfer in such a coherent regime.[20]

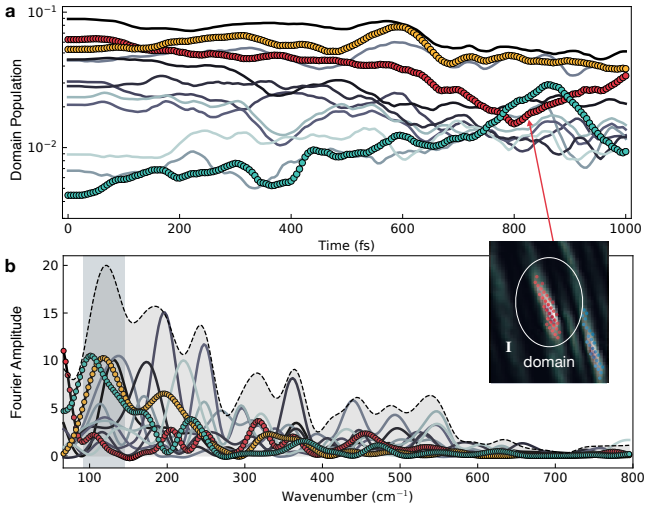

Figure 4.3: Evolution of the domain population $P_{\text{domain}}(t)$, for distinct domains taken from exciton states at 0, 600 and 865 fs for the $\hat{H}(t)$ case, showing a clear oscillatory behavior. (a) Domain population along the 1 ps exciton dynamics trajectory. (b) Fourier spectra (amplitude versus wavenumber) calculated from the time traces of the domain populations. The light gray rectangle highlights the frequencies between 91 cm^{-1} and 145 cm^{-1}. Domain I,II and III are highlighted by red, yellow and green colors. Frequencies corresponding to time scales longer than half of the exciton trajectory of 1 ps are not shown.

Site Basis Population Modulation. As demonstrated in FMO studies,[22,23] periodic modulation of the population in the site basis along the exciton dynamics trajectory characterizes quantum beatings that have been detected by 2DES. We investigate the population variation to determine periodic modulations that match coherent beatings measured in chlorosomes systems, *e.g.* at 91 and 145 cm^{-1}.[84] As domains of high exciton population are formed due to strong electronic coupling between pigments in chlorosomes, we determined the population evolution over domains instead of over individual sites, *i.e.* via the total population in a domain, $P_{\text{domain}}(t)$ defined as

$$P_{\text{domain}}(t) = \sum_{\text{site } i \in \text{domain}} \rho_{ii}(t) \tag{4.6}$$

where ρ_{ii} is the population on site i. Figure 4.3 summarizes the $P_{\text{domain}}(t)$ for the considered domains. To capture significant domains at the early and late stages of exciton evolution, we considered domains determined from snapshots at 0, 600 and 865 fs (see Figure 4.2b). For clarity, $P_{\text{domain}}(t)$ for the domains labeled I, II and III in Figure 4.2b are highlighted and more details are provided in the Appendix C (see Figure C.4 for how domains are defined and their $P_{\text{domain}}(t)$ plots).

Oscillatory behavior of the domain population P_{domain} is observed for all domains, see Figure 4.3a, which cannot be explained in terms of monomeric properties but suggest many weak coherences along the exciton dynamics trajectory. In particular, the frequency of these oscillations can be quantified by spectral analysis of the P_{domain} time traces, see Figure 4.3b. Concentrating on the range where quantum beats are experimentally observed, *i.e.* 91 cm^{-1} and 145 cm^{-1} (light gray area in Figure 4.3b), we find that the average intensity is maximal, with high-population domains (II and III) showing also a maximum intensity. This match between the periodicity of P_{domain} modulation and experimentally observed coherent beats suggests that quantum beats can also be induced by the ground state nuclear dynamics, in line with the observation in a recent study about FMO.[156] We note that, the P_{domain} variation in the $\hat{H}_1$ case is much weaker, as shown in Figure C.5, and the Fourier spectra are less rich. In particular the maximum intensity is found around 200 cm^{-1}.

Although the exciton evolution is determined by variation of the Hamiltonian of the whole system, we tried to identify microscopic signatures of the dynamic

disorder in the domains that can be correlated to their population oscillations. We first calculated the overall coupling strength J_{domain}, see definition in Appendix C. We observe a clear correlation between J_{domain} and P_{domain} (Figure C.6): higher domain population corresponds to stronger coupling J_{domain}. The calculated cross-correlation values between J_{domain} and P_{domain} for the domain I, II and III are −0.61, −0.34, and −0.21 respectively, which shows that they are correlated. This is further supported by the distribution of cross-correlation distribution for all considered domains, see Figure C.7a. To see if there is a direct relation between earlier identified simple structural modes, like rotation (average relative rotation angle α) and lattice vibrations (average distance d between neighboring transition dipoles), and the oscillations of P_{domain}, we analyzed their correlations to P_{domain} as well, see details in Appendix C. We find, see Figure C.7, that their cross-correlations are dispersed, showing that there is no clear direct correlation. Yet, a clear correlation can be identified for J^{-}_{domain}, the negative part of J_{domain}. This indicates that oscillation of domain population can not be singled out to a particular structural mode, but are rather due to collective motion inside the domains.

Density Matrix in State Basis. Features of the non-stationary propagation, such as the variation in population and coherence in the state basis, can be investigated by visualizing the diagonal and off-diagonal terms in the density matrices $\rho^{\phi}(t)$ along the exciton trajectory, see Movie S3[†]. In the movie, we only focus on the $k < 350$ part of the density matrix, which covers all the states of significant population: $\rho^{\phi}_{kk} > 10/N (N = 4547$ which is the total number of sites, see Figure C.8). We refer to Figure C.9 for the snapshot at 200 fs and details of our visualization method. Along the exciton dynamics, the exciton mixes from the initial pure state ($k = 20$) with other states in a close energy range. We note that for states $k < 350$, the energy range is approximately 350 cm^{-1}. As observed in the movie S3, coherences between the initial state and other states are built, especially in the later stages when dynamic disorder introduces more significant variation to the initial Hamiltonian. As discussed in Chapter 3, the eigenstates from $\hat{H}(t = 0)$ to $\hat{H}(t)$ may change. To make sure that the coherences between states in the reference state basis shown in the density matrix $\rho^{\phi}(t)$ is not due to a simple switch of eigenstates, we also analyzed the density matrix $\rho^{*}(t)$ in terms of the state basis of the time-dependent Hamiltonian $\hat{H}(t)$, see details in Scheme C.1. As shown in Movie S4[†], consistent with $\rho^{\phi}(t)$, similar

even stronger population variation and introduction of coherences are observed in $\rho^*(t)$. In particular, we observed substantial coherences $\rho^*_{ij}(t)$ on a time scale < 100 fs, *e.g.* see $\rho^*(t = 20$ fs). This indicates that the dynamic disorder in $\hat{H}(t)$ is sufficient to overcome quantum dephasing and to drive semi-classical exciton transfer.

The enhancement of exciton dynamics by dynamic disorder is further demonstrated in the state basis by the analysis of the mean square displacement $\text{MSD}_k = \sum_k \rho^{\phi}_{kk}(t)(k - k_0)^2$ in the reference state basis $|\phi_k\rangle$. Using $\text{MSD}_k \propto Dt$, the extracted diffusion coefficient D in the $\hat{H}(t)$ case, $D_t = 21.983$ fs^{-1}, is about four orders of magnitude larger than $D_1 = 0.002$ fs^{-1} for $\hat{H}_1$, see Figure 4.4a. Consistent with our analysis of the exciton dynamics trajectories in real space, exciton transport in state basis is limited for the static $\hat{H}_1$ case, where the exciton state is trapped in the initial state. In the dynamic $\hat{H}(t)$ case, however, exciton transport in state basis is facilitated by the dynamic disorder that stems from the thermal energy.

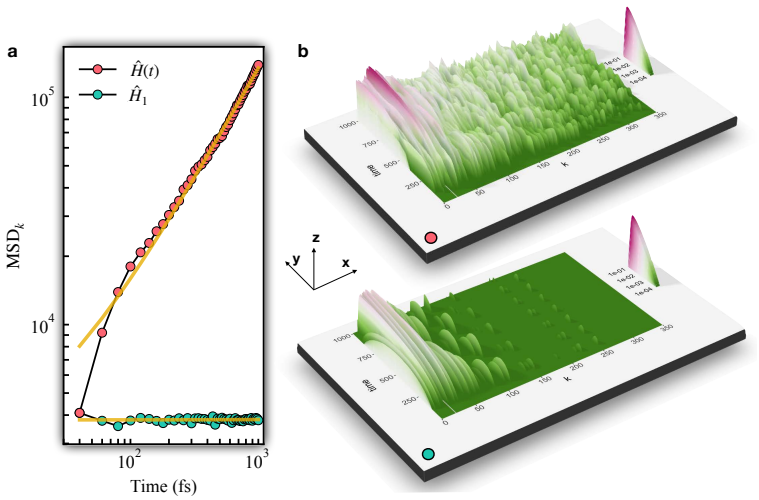

Figure 4.4: Enhancement of exciton dynamics in state basis due to dynamic disorder obtained from MD. (a) Comparison of the MSD_k in the reference state basis for two cases: the dynamic $\hat{H}(t)$ and static $\hat{H}_1$. (b) 3D plots of the population ρ^{ϕ}_{kk} in the state basis $|\phi_k\rangle$ (z-axis) as a function of state number k (x-axis) and time t (y-axis), top for $\hat{H}(t)$ and bottom for $\hat{H}_1$.

Landscape. We may further analyze these results by considering the time traces of populations in the reference state basis for all states $k < 350$, via the 3D plots in Figure 4.4b. From the $\hat{H}(t)$ case, Figure 4.4b top, it is clear that thermal energy creates a fluctuating (potential) energy landscape for the exciton, which drives migration in the states basis and enhances mixing of exciton states. Without accumulation of perturbations due to thermal fluctuation, in the $\hat{H}_1$ case (Figure 4.4b bottom), the exciton dynamics is much simpler, with well-defined oscillations resulting from fixed phase factors in the coherence terms. Animations for different perspectives of the 3D plots for the two cases are given in Movie S5 and Movie S6.[†]

Multi-tube. As experimental imaging shows that chlorosomes consist of hierarchical tube structures,[37] we also conducted exciton dynamics simulations on two types of hierarchical assemblies: concentric tubes (3 nested tubes) and side-by-side aligned tubes (2 tubes). We focused on the question how the inter-tube connectivity affects the exciton transfer. Figure C.10 shows simulation details and our analysis of the initial state survival probability P_S as well as the tube population $P_{\text{tube}}(t) = \sum_{\text{site } i \in \text{tube}} \rho_{ii}(t)$ along the exciton trajectories. As characterized by P_S, the enhancement of exciton transfer by dynamic disorder is also present in both the multi-tube cases. By comparing P_{tube} for both multi-tube topologies, we find stronger inter-tube fluctuations in the concentric tube case and P_{tube} reaches equilibrium faster, reflecting a stronger inter-tube electronic coupling in the concentric tube topology. The inter-tube transfer time scale, *i.e.* the time that P_{tube} reaches equilibrium, is about 4 ps (concentric tube) to 10 ps (aligned tubes), which is longer than the intra-tube transfer time scale of 1 ps. This result suggests that prior to energy annihilation at a timescale of 10 ps,[61] an exciton is able to migrate across different layers in concentric tubes and across separate tubes.

For the different tube radii R in the concentric tube case, the equilibrium P_{tube} increases with increasing radius R, in line with our previous static analysis that there is a biased transfer from inner to outer tube due to the geometric condition that larger tubes contain more molecules with $N \propto R^2$ (Chapter 3). In particular, when *syn-anti* packing units assemble into tubes, their hydrophobic farnesyl tails will cover both the inside and outside of each nested tube, which provides the option of forming tightly packed concentric tubes (Chapter 2). Compared with the side-by-side tube topology, the inter-tube exciton dynamics

is enhanced and biased towards to the outer tube in the concentric tube topology, which is more favored in terms of the efficiency in the whole energy transfer process.

How can we relate our computational results to natural chlorosomes? In nature, chlorosomes are oblong-shaped assemblies of complete and incomplete concentric tubes, with an overall dimension that is generally smaller than the wavelength of the absorbed light.[34,157] It therefore makes sense to assume that incident light will excite an eigenstate that is delocalized over the entire chlorosome, see the results in this subsection, albeit that high exciton populations will again be confined to small domains that are scattered over the whole structure. In particular, since the total population in each of the concentric tubes is found to scale with the number of constituting pigments at longer times, we may conclude that the intra-tube excitonic features are rather independent of the tube radius. Thus, they are likely to agree with that of a single tube.

The EET, however, can be seen to depend on the inter-tube connectivity, with a more efficient exciton transfer in concentric than in side-by-side tubular assemblies. Yet, since chlorosomes are known to assemble via a nucleation and growth process,[100] it is unlikely that such functional requirements prescribe the actual tube connectivity in natural chlorosomes. It is more likely that energy transfer to a "sink" like the baseplate starts directly after excitation, and that mixing of exciton states due to the dynamic disorder from nuclear motions plays a more dominant role in EET than the actual inter-tube connectivity.

4.4. Conclusion

The essential requirement for utilizing thermal energy to enhance the exciton transfer is that the strength of dynamic disorder, associated with thermal motions, is comparable to the energy gaps between exciton states.[20] If the energy gaps are too large or the dynamic disorder too weak, migration in the state basis will be limited, as been illustrated for the static case $\hat{H}_1$. Liquid crystalline materials composed of densely packed pigments, for instance, chlorosomes and carbocyanine dye nanotubes, are suitable for high-efficient long-distance EET since these requirements are easily met: 1) the presence of a large number of pigments expressing structural disorder guarantees a large number of exciton

states of very similar energy; 2) the relative low energetic costs of pigment rotation in the tube due to thermal motion, even in dense packing, gives rise to rotation of transition dipoles or dynamic disorder. This is in contrast to the situation where pigments are confined in a protein matrix, where disorder mainly stems from the environment in which pigments are trapped; 3) the fluctuating nature of the dynamic disorder, at several lengths and time scales, prevents trapping in eigenstates, for instance low energy states, and promotes efficient exciton transfer, in line with a recent 2DES study.[121]

By including the pigment assembly dynamics stemming from ground state molecular dynamics at room temperature in the fluctuating electronic coupling terms of our Frenkel Hamiltonian, we have been able to study the role of dynamic disorder in enhancing the exciton transfer. We observed several phenomena that are in line with experimental observations, despite the simplifications considered in our approach. It can be anticipated that methodological improvements within the computational concept,[73,158] for instance, site-dependent site energy and more precise methods for the electronic coupling, will only strengthen our main conclusions.

In chlorosomes, local molecular motion is a key property. It is a generic property for structures composed of head-head packing unit, and independent of the particular molecular component (or BChl pigment), the hierarchical nature of the structure (close/open tubular or planar), or overall size. Simple but general, dynamic disorder that originates from these local molecular motions is capable of inducing a fluctuating landscape for the excitons, which enhances exciton transfer. Our findings are a key step towards solving the long-lasting puzzle about why efficient exciton transfer is widely observed in different types of chlorosomes and other light-harvesting complexes. Following this principle, we also suggest that the liquid-crystal like aggregates assembled from pigments with some sort of symmetry breaking, for instance, chlorosomes and the carbocyanine dye nanotubes, all rely on the same principle for efficient long-distance energy transfer.

4.5. Acknowledgments

The authors acknowledge Prof. dr. A. R. Holzwarth for helpful discussions. The use of supercomputer facilities was sponsored by NWO Exact and Natural Sciences, with financial support from the Netherlands Organization for Scientific Research (NWO).